International Journal of Nanomedicine

Dovepress
open access to scientific and medical research

Open Access Full Text Article

ORIGINAL RESEARCH

pH/Redox Dual-Responsive Drug Delivery System with on-Demand RGD Exposure for Photochemotherapy of Tumors

Yaning Li[1], Junfang Nie[1], Jie Dai[1], Jun Yin[1], Binbin Huang[1], Jia Liu[1], Guoguang Chen[1], Lili Ren[1,2]

[1]School of Pharmacy, Nanjing Tech University, Nanjing, People's Republic of China; [2]Department of Microbiology and Immunology, Stanford University, Stanford, CA, USA

Correspondence: Guoguang Chen; Lili Ren, School of Pharmacy, Nanjing Tech University, Nanjing, People's Republic of China, Tel +86-2558-139-416, Email ggchen@njtech.edu.cn; renlili@njtech.edu.cn

Purpose: Nanotechnology has been widely used in antitumor research. The complex physiological environment has brought significant challenges to the field of antitumor micelles. The ideal micelles must not only have an invisible surface to extend the circulation time but must also enhance the retention of drugs and cellular internalization at the tumor.

Methods: A graded response micelle (RPPssD@IR780/DOC) was designed to self-assemble by cRGD-poly(β-amino esters)-polyethylene glycol-ss-distearoyl phosphatidylethanolamine (cRGD-PBAE-PEG-ss-DSPE) loaded with docetaxel (DOC) and IR-780 iodide (IR780). The micelles were designed to allow the PEG shell to prolong the blood circulation time in the body and effectively accumulate in the tumor. Subsequently, the acidic microenvironment of the tumor could transform the PBAE to hydrophilic, thereby increasing the size of micelles and exposing cyclic Arg-Gly-Asp (cRGD) peptides to increase the retention and cellular internalization of micelles in the tumor. After tumor cells had captured micelles, the high expression of glutathione in the cells prompted the release of DOC and IR780. Subsequently, the IR780 was stimulated by an 808-nm laser to generate local heat and reactive oxygen species (ROS) to synergize with DOC to treat the tumor.

Results: In vitro and in vivo experimental results suggested that RPPssD@IR780/DOC was a potential photochemical effective for the treatment of tumors with non-negligible antitumor activity and good biocompatibility.

Conclusion: A dual-response pH/redox delivery system with on-demand RGD exposure was designed to achieve photochemotherapy of tumors with good biosafety and antitumor effects.

Keywords: micelles, drug delivery, ligand hidden, size variable, photo-chemotherapy

Introduction

Cancer is the second leading cause of human death and has shown an increasing trend year by year, seriously threatening the development of human health and the social economy.[1] Conventional cancer treatment options include chemotherapy, radiotherapy, and surgery.[2] However, chemotherapy generally leads to serious side effects, surgery is accompanied by a high tumor recurrence rate, and radiotherapy is limited by the therapeutic dose. These methods are unable to achieve satisfactory results on cancer.[3] To solve the above problems, the combination of chemotherapy with other antitumor therapies represents a potential treatment method, the use of multiple treatments can effectively stimulate the benefits and decrease the side effects of chemotherapy drugs.

Recently, complementary anticancer therapies, photodynamic therapy (PDT) and photothermal therapy (PTT), have been applied alone or in combination with traditional methods to enhance efficacy and reduce side effects.[4] PTT or PDT is an antitumor therapy that uses laser irradiation of photosensitizer (PS) enriched in the tumor area to generate local hyperthermia or a large amount of cytotoxic reactive oxygen species (ROS) to induce cell apoptosis or necrosis.[5,6] Photosensitizers that are not excited by exogenous light have minimal toxicity. Additionally, PDT and PTT acts only on the lesion tissue in the irradiated area, which can significantly improve the targeting of tumor treatment and reduce the

Received: 14 September 2022
Accepted: 15 November 2022
Published: 23 November 2022

Graphical Abstract

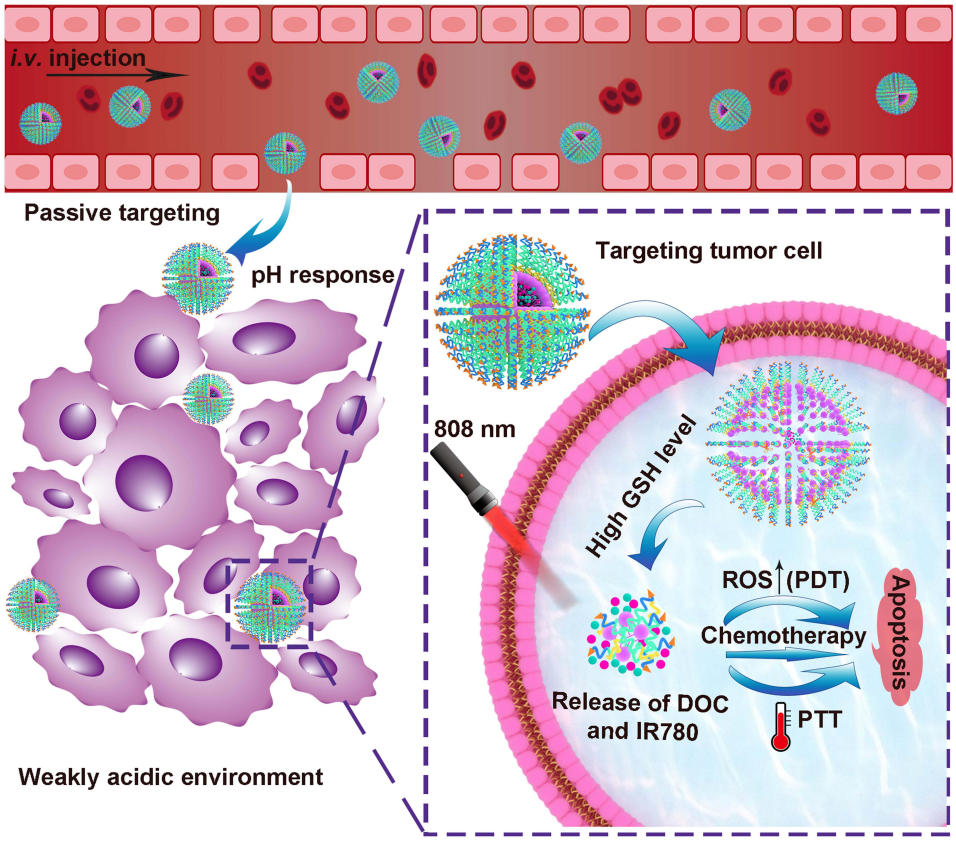

toxic side effects that can be caused by traditional chemotherapy and radiotherapy.[7,8] However, the low water solubility and low tumor specificity of photosensitizers limit their clinical application.[9] In this context, establishing a micelle that can enhance the solubility of the PS and deliver it precisely to the tumor site is particularly important for PDT and PTT applications.[10]

Given the rapid advances in nanotechnology, the micelle has been widely proposed for the delivery of antitumor drugs due to its small size, easy modification and good solubility.[11] The enhanced permeability and penetration (EPR) effect caused by rapid proliferation of tumor cells and restricted lymphatic circulation in tumor tissue is tumor-specific, and is often used for targeting tumors with micelles.[12] As research progresses, it is not enough to rely solely on passively targeted delivery of drugs to tumor sites. The accumulation of micelles in tumor tissues greatly affects the efficacy of drugs. Many studies have found that micelles larger than 200 nm tend to remain longer in tumor tissue than smaller particles.[13,14] In addition, the strategy of modifying specific ligands on the surface of micelles while taking advantage of the characteristics of the tumor microenvironment (micro-acidic environment, highly expressed enzymes, and redox environment) to control drug release has shown great potential in improving the efficiency of tumor targeting.[15–17] However, evidence is mounting that after entering the blood circulation, the micelles will be coated with proteins to form a "protein corona".[18] In this case, even if the micelles have special surface modifications, they will fail quickly after entering the body fluid environment.[19] For instance, cationic micelles were designed to take advantage of the negatively charged properties of cell membranes that can enhance cellular uptake. Contrary to expectations, cationic micelles are more likely to form a protein corona, resulting in a negative overall charge of the micelles, which impedes their uptake by cells.[20] Furthermore, micelles equipped with targeting ligands are also covered by the protein corona, leading to failure of the ligand and off-target effects.[21] To cross this barrier,

a negatively charged polyethylene glycol shell structure was designed to reduce the protein adhesion.[22] Stealth surfaces also reduce the uptake of micelles by cancer cells while avoiding protein adhesion. Consequently, designing a tunable size and stealth surface micelle that enhances tumor accumulation and tumor uptake is critical.[23]

To address the above problem, we developed a tumor microenvironment-responsive micelle with tunable sizes able to target concealable ligands to improve the retention and cellular uptake of micelles in tumor tissue for enhancing the efficiency of cancer therapy. The concealable targeting ligand is achieved by linking to a pH-responsive poly(β-amino ester) (PBAE), which can remain hydrophobic under physiological conditions and convert to hydrophilic in an acidic environment through tertiary amine protonation on the chain. As shown in Figure 1, drug-loaded micelles consist of the target peptide cRGD, pH-responsive hydrophobic PBAE chain, hydrophilic polyethylene glycol (PEG) segment, hydrophobic chain distearoyl phosphatidylethanolamine (DSPE) present good biocompatibility, and is loaded with hydrophobic anticancer drug docetaxel and photosensitizer IR-780 iodide (IR780).[24–26] At physiological pH (≈7.4), both the cRGD-PBAE and DSPE segments were trapped within the hydrophobic core of RPPssD and the targeting peptide cRGD was shielded by the PEG coating, which makes the surface invisible and prolongs the blood circulation time of RPPssD. Once RPPssD the drug reaches tumor tissue (pH<6.8), the PBAE segments undergo a transition from hydrophobic to hydrophilic properties with protonation of the tertiary amino group, allowing exposure of the cRGD peptides of RPPssD. Thus, the size of RPPssD can be increased, and the cRGD peptide can bind to tumor cells, resulting in enhanced tumor retention and cellular internalization of RPPssD. Subsequently, in the presence of intracellular glutathione (GSH), cRGD-PBAE-PEG segments are separated from RPPssD by disulfide bond cleavage to improve the release of DOC and IR780.[27] Finally, the active oxygen and local hyperthermia produced by free IR780 under 808 nm near-infrared (NIR) light irradiation cooperate with DOC to induce tumor cell apoptosis. Overall, the prepared micelles provide a strategy for prolonging blood circulation and improving tumor cell targeting for photochemical treatment of tumors.

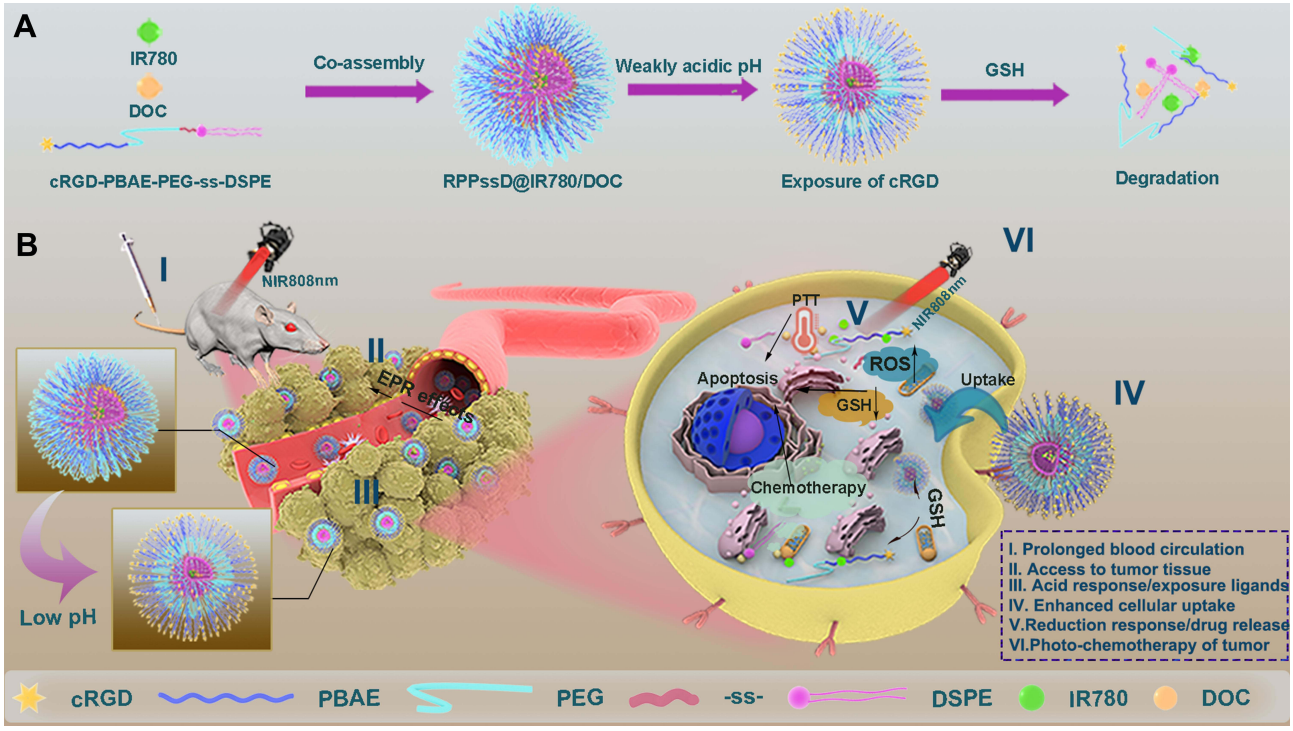

Figure 1 Schematic illustration of RPPssD@IR780/DOC micelles to achieve particle size changes, hide targets, and treat tumor synergistic photochemical combination. (**A**) Formulation, particle size changes, hidden targets, and degradation mechanism of RPPssD@IR780/DOC micelles. (**B**) The tumor-targeted micelles RPPssD loaded with DOC and IR780 to treat tumors through light-triggered photochemotherapy.

Methods

Determination of Critical Micelle Concentration (CMC) of cRGD-PBAE-PEG-ss-DSPE

The CMC of RPPssD was determined using the pyrene fluorescence probe method.[28] An acetone solution with a pyrene concentration of 6×10^{-6} mol/L was prepared and added to aqueous solutions of RPPssD concentrations with 0.05, 0.10, 0.20, 0.50, 1.00, 2.00, 5.00, 10.00, 20.00, 50.00, 100.00, 200.00, 500.00, 1000.00 μg/mL. These solutions were placed in a 37°C water bath and incubated for 1 h in the dark and then protected from light at room temperature overnight. The emission wavelength of the fluorescence spectrophotometer was set to 334 nm. The excitation wavelengths of pyrene were 373 nm and 384 nm, respectively. The width of the slit was 3.0 nm. The fluorescence intensity ratio I_{373}/I_{384} against the logarithmic concentration of RPPssD in the aqueous solution was plotted and the inflection point was the CMC of RPPssD.

Preparation of Micelles

The micelles of RPPssD and RPPssD@IR780/DOC were all prepared by thin-film hydration methods.[29] First, RPPssD was dissolved in acetone. Subsequently, the thin film formed after the solvent was evaporated. The film was hydrated with pH 7.4 PBS and the blank micelles of RPPssD was obtained after the solution passed through a 0.45-μm filter membrane. To prepare RPPssD@IR780/DOC, DOC (1 mg) and IR780 (0.2 mg) were added to the acetone with RPPssD (5 mg) at the beginning of micelles preparation. The remaining steps were the same as those for the preparation of blank micelles.

Characterization of Micelles

The particle size and potential of RPPssD@IR780/DOC were measured using a laser dynamic scatter meter at 25°C. Furthermore, the morphology of RPPssD@IR780/DOC was observed by transmission electron microscope (TEM). In addition, the stability of RPPssD@IR780/DOC under different conditions was evaluated by the particle size and polydispersity index (PDI). Furthermore, the drug loading (DL%) and encapsulation efficiency (EE%) of DOC and IR780 in drug-loaded micelles were determined by HPLC and UV, respectively. As standard, 1 mL of micellar solution was diluted to 10 mL with methanol, sonicated for 30 min and filtered through a membrane syringe filter (0.22 μm). The concentration of DOC was detected by HPLC. The 55:45 (v/v) acetonitrile/water mixture was used as the mobile phase with a flow rate of 1 mL/min and the detection wavelength was 228 nm. The content of IR780 was obtained by detecting the absorption value at 780 nm with a UV. The DL% and EE% values were calculated according to the Eqs (1) and (2):

$$\text{EE}\ (\%) = \frac{\text{Amount of drug entrapped}}{\text{Total amount of drug}} \times 100 \quad (1)$$

$$\text{DL}\ (\%) = \frac{\text{Amount of drug entrapped}}{\text{Total amount of micelles}} \times 100 \quad (2)$$

Furthermore, the saturated solubility of DOC and IR780 in water was detected and photographed to record the dissolution phenomenon.

Evaluation of pH Sensitivity of Micelles

The structure of the synthesized RPPssD contains a protonable tertiary amine group to make it pH sensitive.[30] In order to fully understand the pH-sensitive properties of the material, a series of characterizations was conducted. The acid-base titration method was used to test the buffering capacity of the material to acid by using a pH meter.[31] The particle size of RPPssD was detected by a laser dynamic scattering instrument to describe the variation trend of the particle size of self-assembled micelles with the pH value of the environment. In addition, the morphology of RPPssD micelles at pH 4.5 and pH 6.5 was observed by TEM.

The Effect of Reduction on Micelles

The structural unit of the RPPssD polymer contains disulfide bonds, which are broken in the presence of reducing agents (such as GSH and dithiothreitol [DTT]) and change the properties of the material change.[32] To comprehensively

determine the reduction sensitivity of RPPssD, the trend of the size of the micelles after self-assembly over time and the concentration of the reducing agent was tested using a laser dynamic scatter meter.

Evaluation of the Photothermal Effect in vitro

The photothermal effect of RPPssD@IR780/DOC was measured by an infrared thermal imager. The IR780 solution (30% methanol) with a concentration of 20 μg/mL, free DOC solution and PBS were prepared as a control for RPPssD@IR780/DOC. After adding 1 mL of the solutions to the vial, the sample solution was irradiated with a laser (1 W/cm^2, 808 nm) for 10 min and the temperature of the sample was recorded in each well with an infrared thermal imaging camera every 2 min to plot the temperature rise curve. Additionally, to verify the photothermal stability of RPPssD@IR780/DOC, free IR780 and RPPssD@IR780/DOC containing IR780 at a concentration of 20 μg/mL were irradiated with 808 nm NIR light (1 W/cm^2) for three cycles, each cycle lasted 6 min and the sample temperature was recorded every 2 min to plot the temperature change curve. To calculate the photothermal conversion efficiency (η), RPPssD@IR780/DOC and free IR780 (30% methanol) with IR780 concentration of 20 μg/mL were irradiated with a laser (1 W/cm^2, 808 nm) for 6 min and then cooled naturally for 6 min, and the temperature change was recorded every 20s. The photothermal conversion efficiency was calculated according to Eq (3). Deionized water was set as the control group.[33,34]

$$\eta\ (\%)\ =\ \frac{\mathrm{hs(Tmax\ -\ Tsurr)\ -\ Qdis}}{\mathrm{I}\left(1\ -\ 10^{\ -\ \mathrm{A808}}\right)}\times\ 100 \tag{3}$$

In the formula, η is the photothermal conversion efficiency value, T_{max} is the maximum temperature of the solution after irradiation with NIR light, T_{surr} is the ambient temperature, Q_{dis} the heat emitted from the environment, h is the heat transfer coefficient of the system, s is the surface area of the irradiated solution, I is the power density of the 808 nm laser used, and A_{808} is the absorbance value of the sample at 808 nm.

Evaluation of the Photodynamic Effect in vitro

The 3-diphenylisobenzofuran (DPBF) assay was used to investigate the singlet oxygen generation of RPPssD@IR780/DOC under laser irradiation. DPBF can chemically react with singlet oxygen, which will reduce its absorbance at 418 nm, thus reflecting the situation of singlet oxygen.[35] Next, 250 μL PBS, free DOC, free IR780 (20 μg/mL) and RPPssD@IR780/DOC solution were added to 96-well plates, followed by the addition of 50 μL DPBF solution (50 mM) to each well. Each well was irradiated with an 808-nm laser (1 W/cm^2) for 1, 2, 3, 4, 5, 6, 7, 8, 9, 10 min and the absorbance at 418 nm of the sample was measured with a microplate reader.

Drug Release of RPPssD@IR780/DOC Under Different Conditions

Six equal volumes (1 mL) of RPPssD@IR780/DOC solution were placed in dialysis bags (MWCO: 3500 Da). And then put them into a 50-mL release tube containing 30 mL of different release mediums (pH7.4, 6.8, 5.0,7.4+10 mM DTT, 6.8 +10 mM DTT, 5.0+10 mM DTT). Three parallel samples were set for each group.[36–38] All release tubes were placed in a constant temperature shaking box at 37°C, set the vibration amplitude to 100 rpm. According to the predetermined time (10 min, 20 min, 30 min, 45 min, 1 h, 2 h, 4 h, 6 h, 8 h, 12 h, 24 h, 48 h, and 72 h), 1 mL release solution was taken and an equal volume of release medium was added at the same time. After obtaining all samples at each time point, the degree of release of DOC and IR780 in different media was measured by HPLC and UV spectrophotometer and the cumulative release curves were drawn.

Hemolysis Test

After collecting 5 mL of fresh rabbit blood, the serum was removed by centrifugation at 1000 rpm for 10 min. The red blood cells obtained after washing five times with PBS were prepared into a 2% red blood cell suspension for later use. A solution of RPPssD@IR780/DOC with an RPPssD concentration of 15 mg/mL was prepared. 2.5 mL of red blood cell suspension was mixed with RPPssD@IR780/DOC micelles solution (0.1, 0.2, 0.3, 0.4, 0.5 mL) and normal saline (2.4, 2.3, 2.2, 2.1 mL), respectively. A negative control group (2.5 mL of erythrocyte suspension with 2.5 mL of normal saline)

and a positive control group (2.5 mL of erythrocyte suspension with 2.5 mL of deionized water) were prepared and incubated samples of different components at 37°C for 3 h. The samples were then centrifuged and photographed and 100 μL was taken from each different group to measure the optical density (OD value) at 540 nm with a microplate reader. The hemolysis rate was calculated by Eq (4).

$$\text{Hemolysis } (\%) = \frac{\text{ODsample} - \text{ODcontrol}}{\text{ODpositive} - \text{ODnegative}} \times 100 \quad (4)$$

Cytotoxicity Analysis of RPPssD

The cell counting kit-8 (CCK-8) was used to determine the cytotoxicity of blank RPPssD micelles to MDA-MB-231 and L02 cells. Cells were seeded in a 96-well plate at a density of 5×10^3 cells per well and incubated overnight. The concentration of RPPssD was 10 to 1000 μg/mL and incubated with different cells for 24 h. PBS was used as a negative control group. Subsequently, the medium was replaced by fresh medium containing 20 μL CCK-8 solution and incubated at 37°C for 1 h. Finally, a microplate reader was used to measure the absorbance at 450 nm of each well. Relative cell viability (%) was calculated using Eq (5):

$$\text{Cell viability } (\%) = \frac{\text{Asample} - \text{Ablank}}{\text{Acontrol} - \text{Ablank}} \times 100 \quad (5)$$

In the formula, the A_{blank} is the absorbance value containing only the medium at 450 nm, the $A_{control}$ is the absorbance value of the untreated cell group at 450 nm and the A_{sample} is the absorbance value of each experimental group at 450 nm.

Cellular Uptake

The fluorescence of IR780 was used to evaluate the ability of micelles to enter cells. The cellular uptake of free IR780, RPPssD@IR780 at pH7.4 has been explored. Additionally the cellular uptake of free IR780 and RPPssD@IR780 at pH6.8 was also investigated. MDA-MB-231 cells with high expression of the RGD receptor and MCF-7 cells with low expression of the RGD receptor were selected for research.[39–41] Both cells were seeded in a six-well plate at a density of 3×10^5 and cultured for 24 h. The medium containing IR780 or RPPssD@IR780 (the amount of IR780 in each group was 5 μg/mL) were used to replace the original medium. Each group was cultured in an incubator for 6 h. Subsequently, the culture medium was discarded and the extracellular free drug was washed thoroughly with PBS. Subsequently, the nuclei were stained with Hoechst 33,342 for 15 min. Finally, the excess staining solution was washed off with PBS and the fluorescence picture of the cells was taken with an inverted fluorescence microscope.

Cellular ROS Generation

We used 2′,7′-Dichlorofluorescin diacetate (DCFH-DA) as the reactive oxygen probe to detect the level of reactive oxygen after laser irradiation of free IR780 and RPPssD@IR780 micelles at pH 7.4. The level of active oxygen production of free IR780 and RPPssD@IR780 at pH 6.8 was also investigated using laser irradiation. PBS and its laser irradiation groups were used as control. The MDA-MB-231 cells in the logarithmic growth phase were seeded on a 12-well plate at a density of 6×10^4 per well and cultured overnight until the cells adhered. Subsequently, the old medium was replaced with a medium containing PBS, IR780, RPPssD@IR780 (IR780=5 μg/mL). The cells were incubated for 6 h. Furthermore, the free sample solution was washed with PBS and 1 mL DCFH-DA medium was added to each well. After incubation for 30 min in the dark, the old medium was discarded, and the same amount of fresh medium was added. After 6 minutes of laser irradiation (808 nm, 1 W/cm^2), the culture medium was discarded. The cells were stained with Hoechst 33,342 staining solution and then washed with PBS to remove the excess staining solution. Finally, the 12-well cell culture plate was placed under a fluorescent inverted microscope to observe the fluorescence signal of each well and photographs were taken.

In vitro Antitumor Activity

The antitumor activity of free drugs, RPPssD@IR780/DOC were detected using the CCK-8 assay. MDA-MB-231 cells with high expression of the RGD receptor and MCF-7 cells with low expression of the RGD receptor in the logarithmic

growth phase were seeded in a 96-well plate at a density of 5×10^3 cells/well and cultured overnight. A RPPssD@IR780/DOC group and the free DOC/IR780 group at pH7.4 with or without laser irradiation were established to investigate viability in tumor cells. Furthermore, viability in tumor cells of RPPssD@IR780/DOC and free DOC/IR780 at pH 6.8 with laser was also detected. The concentration of DOC was adjusted to 0.001–40 μg/mL and the amount of DOC was five times higher than that of IR780. The cells in the laser group were irradiated with laser (808 nm, 1 W/cm^2, 6 min) 6 hours after administration. In addition, PBS was used as a negative control group. After incubating the cells of all experimental groups for 24 h, 20 μL CCK-8 reagent was added to each well and incubated at 37°C for 1 h. Subsequently, the microplate reader was used to detect the absorbance value of the sample in the 96-well plate at 450 nm. Cell viability was calculated by Eq (4).

The Live/dead staining assay was used to further evaluate the antitumor effect of free drugs and RPPssD@IR780/DOC with or without laser at pH 7.4. The antitumor effects of free drugs and RPPssD@IR780/DOC at pH6.8 with laser were also investigated and PBS was used as a control group. According to the density of 6×10^4 cells per well, MDA-MB-231 was seeded in 12-well plates and cultured overnight until cells adhered. The old medium was replaced with the medium containing PBS, IR780/DOC, RPPssD@IR780/DOC, and the culture was continued for 24 hours. At 6 h after administration, the group that needed the laser was irradiated with a 1 W/cm^2 laser (808 nm) for 6 minutes. Finally, calcein-AM/PI was added for staining. After incubation was completed, the apoptosis of MDA-MB-231 cells was evaluated by a fluorescent inverted microscope.

Examination of in vivo Photothermal Effects

Tumor-bearing mice with tumor volumes up to about 100–150 mm^3 were randomly divided into three groups and administered saline, DOC/IR780, and RPPssD@IR780/DOC respectively by tail vein. Administered at 10 mg/kg (DOC/body weight) and 2 mg/kg (IR780/body weight). Eight hours after the tail vein injection, the tumor surface area of the tested mice was irradiated with laser (808 nm, 1 W/cm^2) for 6 minutes. During irradiation, the tumor surface temperature and tumor area were photographed with the infrared thermographer every 2 min.

In vivo Photochemotherapy for Tumors

Tumor-bearing mice with tumor volumes of 100–150 mm^3 were randomly divided into five groups (n=6): (A) Control group (saline); (B) Control+Laser (saline+Laser) group; (C) Free DOC/IR780 group; (D) Free DOC/IR780+Laser group; (E) RPPssD@IR780/DOC group; (F) RPPssD@IR780/DOC+Laser group. The mice received a tail vein injection at a dose of 10 mg/kg (DOC/body weight) and 2 mg/kg (IR780/body weight) once every 3 days, six times in total. The laser groups were irradiated with an 808-nm laser (1 W/cm^2, 6 min) at the tumor site 8 h after administration. The tumor volume and body weight the mice were measured every 2 days. On the third day after the last treatment, mice were killed and tumors and major organs (heart, liver, spleen, lung, and kidney) were collected. The tumors in each group were weighed and photographed. Subsequently, H&E staining and Ki67 staining were performed on tumors in each group to further observe the antitumor effects. Furthermore, the biological safety of RPPssD@IR780/DOC was evaluated by histological analysis of the major organs of mice after H&E staining and combined with the results of routine and biochemical blood analyses in each group of mice. Mice with a tumor volume of 100–150 mm^3 were treated according to the same experimental protocol as above and the survival of each group of mice was recorded and the survival curve was plotted.

Statistical Analysis

Experimental data were expressed as mean ± standard deviation and analyzed by two-sided *t*-test (Student's *t*-test) using GraphPad Prism software. Differences were considered statistically significant with p-values <0.05.

Results and Discussion

Preparation and Characterization of Micelles

The synthesis method of RPPssD (Figure S1) was detailed in the supporting information and its structure was verified by hydrogen NMR spectroscopy (Figures S2–S6) and gel permeation chromatography (Figure S7), which confirmed the

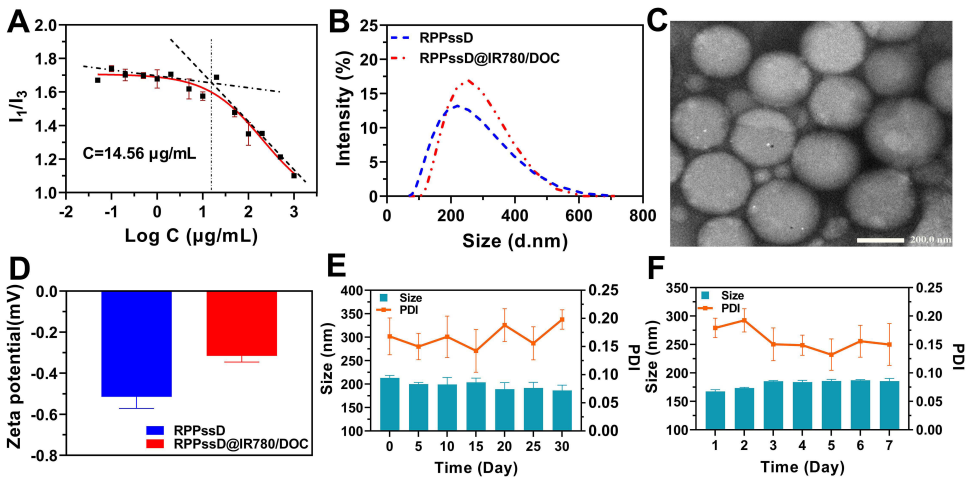

Figure 2 Characterization of RPPssD NPs. (**A**) The CMC of cRGD-PBAE-PEG-ss-DSPE. (**B**) The hydrodynamic diameter of RPPssD@IR780/DOC and the blank micelles of RPPssD. (**C**) TEM image of RPPssD@IR780/DOC (Scale bar=200 nm). (**D**) Zeta potential of RPPssD@IR780/DOC and blank micelles of RPPssD. (**E**) The size and PDI of RPPssD@IR780/DOC in PBS for 30 days. (**F**) The size and PDI of RPPssD@IR780/DOC medium containing 10% fetal bovine serum for 7 days. Data are presented as mean ± standard deviation (n = 3).

synthesis of RPPssD. Before the micelles were prepared, the CMC of the RPPssD was measured using the pyrene fluorescence probe method to be 14.56 μg/mL, which indicated that the RPPssD could form stable micelles in water at lower concentrations (Figure 2A). Subsequently, RPPssD self-assembled IR780 and DOC by the thin film dispersion method to obtain drug-loaded micelles. Similarly, the blank micelles of RPPssD were also prepared by the film dispersion method. The percentage of EE% of RPPssD for IR780 and DOC was calculated using a standard curve (Figure S8), and were 58.11% and 49.10%, respectively. The DL% of RPPssD on IR780 and DOC were 2.07% and 8.76%, respectively. Furthermore, the saturated solubilities of free DOC and IR780 were 1.563 μg/mL and 0.075 μg/mL, respectively, while the amounts of DOC and IR780 in RPPssD@IR780/DOC were 49.1 μg/mL and 11.622 μg/mL, respectively. The results (Figure S9) showed that RPPssD could effectively improve the solubility of DOC and IR780 after encapsulation and the imaging of the dissolution phenomenon also supported the conclusion. As described in Figure 2B, the hydrodynamic diameter of RPPssD@IR780/DOC was 207.3±15 nm and the PDI was 0.11, while the blank micelles size of RPPssD was 182.4±4.67 nm with the PDI was 0.256. This is because the drug has entered the cavity of the hydrophobic segment of RPPssD. TEM clarified that the obtained RPPssD@IR780/DOC micelles were spherical with a particle size of 206.7 ±9.18 nm, which did not differ markedly from the particle size measured by dynamic light scattering (Figure 2C). In addition, the slight negative charge (Figure 2D) on the surface of RPPssD@IR780/DOC was beneficial to prolong blood circulation time and increase the accumulation of tumor. Moreover, RPPssD@IR780/DOC showed excellent stability in PBS or medium containing 10% fetal bovine serum, which ensured the drugs will not leak before it reaches the tumor site (Figure 2E and F).

Evaluation of pH and Reduction Sensitivity of Micelles

To confirm the pH sensitivity of RPPssD, the blank micelles of RPPssD was added to PBS at pH 4.0, 4.5, 5.0, 5.5, 6.5, 7.0, 7.5 and 8.0 for 30 min and then the particle size was measured with dynamic light scattering. As can be seen in Figure 3A, the size of the RPPssD micelles was 178.2±2.1 nm when the pH>7.4. Between pH 7.4 and 5.5, the size of RPPssD obviously increased with the highest size reaching 523.3±23.2 nm. With a pH<5.5, the size of RPPssD no longer increased and remained at 360±20nm. The presence of tertiary amine groups containing PBAE in the RPPssD block polymer explained this result. When the pH was 7.4–5.5, the tertiary amine groups in PBAE were protonated, switching them from hydrophobic to hydrophilic micelles. As a result, the size of RPPssD was expanded and prevented the micelles from returning to the bloodstream to achieve enhanced intratumoral retention. When the pH was <5.5, the protonation of the tertiary amine group in PBAE was close to saturation, so the particle size remained stable, while the decrease in particle size may be caused by the acidolysis of the ester bond in the PBAE of RPPssD. As shown in Figure 3A, the TEM

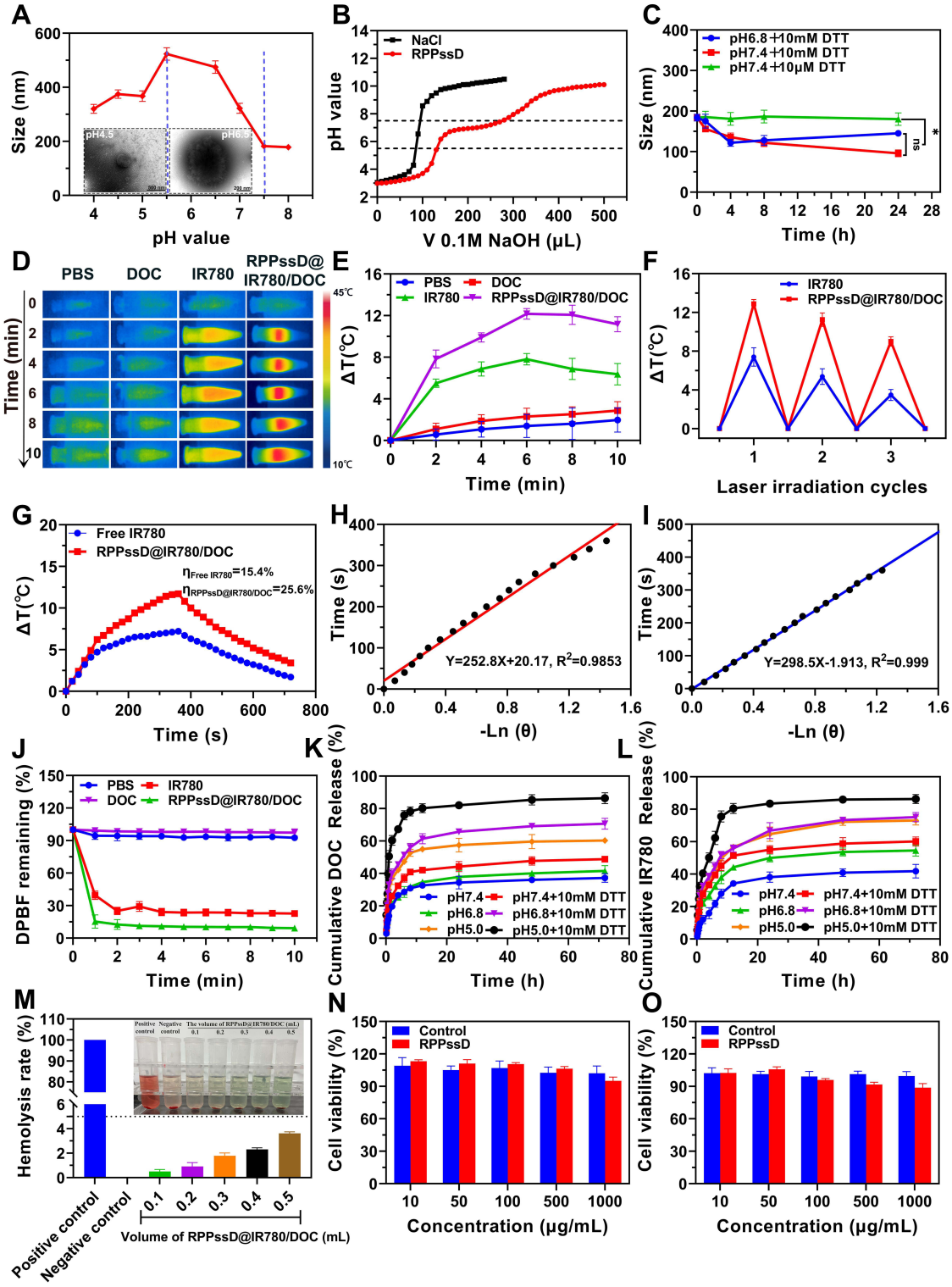

Figure 3 Performance evaluation of RPPssD NPs. (**A**) Variation curves of RPPssD particle size at different pH values and TEM of RPPssD at pH 4.5 (Scale bar=500 nm) and 6.5 (Scale bar=200 nm). (**B**) Acid-base titration curve of RPPssD. (**C**) The curve of RPPssD NP size changes with time at different concentrations of DTT. (**D**) Infrared thermogram of each sample solution after NIR irradiation. (**E**) Temperature change curves of each sample solution under NIR irradiation. (**F**) Temperature change curves of free IR780 and RPPssD@IR780 after 3 cycles of laser irradiation. (**G**) Temperature rise and fall curves of IR780 and RPPssD@IR780/DOC aqueous dispersion. (**H**) The linear time data versus –lnθ obtained from the cooling period of free IR780. (**I**) The linear time data versus –lnθ obtained from the cooling period of RPPssD@IR780/DOC. (**J**) The remaining amount of DPBF after 10 minutes of laser irradiation for different samples. (**K**) DOC-release curves from RPPssD@IR780/DOC at varying conditions. (**L**) Release curves of the IR780 from RPPssD@IR780/DOC at varying conditions. (**M**) The hemolysis rate and experimental hemolysis phenomenon of RPPssD. (**N**) Cell viability of MDA-MB-231 cells after treatment with RPPssD. (**O**) Cell viability of L02 cells after treatment with RPPssD. Data are presented as mean ± standard deviation (n = 3), ns > 0.05, *p < 0.05.

of RPPssD in solutions at pH 4.5 and 6.8 also demonstrated the conclusion. The results show that the particle size of RPPssD at pH 6.5 was about 500 nm and the morphology of PBAE after hydrophobic transformation could be seen. In addition, the particle size of RPPssD at pH 4.5 was about 300 nm and the micelles showed degradation. These results confirm the pH-sensitive properties of RPPssD.

The acid responsiveness of RPPssD was further investigated through acid-base titration. As shown in Figure 3B, compared with the titration curve of the NaCl solution, that of RPPssD changed more gently without a sharp decline, which further indicated that the tertiary amine contained in the PBAE of RPPssD could absorb H^+ and be protonated during the titration process. This proved RPPssD had a pH buffering capacity in the range of pH=5.4–7.4, which was consistent with the effect of pH on particle size. The pH buffering capacity in this range corresponded to the physiological environment and the pH in the tumor tissue, indicating that RPPssD could effectively absorb H^+ in this pH value range to achieve the transition of hydrophilicity and hydrophobicity.

The reductive response of RPPssD micelles was also evaluated (Figure 3C). The size of RPPssD in an environment that simulated normal cells (pH 7.4+10 μM DTT) had no obvious change and was always maintained at about 183.8 ±2.74 nm. As the environment changed to pH 7.4+10 mM DTT, the size of RPPssD changed from 183.8±8.2 nm to 95.8 ±8.33 nm after 24 h, which was caused by the rupture of the disulfide bond in RPPssD after the reduction of DTT. Similar to the condition of pH 7.4+10 mM DTT, the particle size of RPPssD also showed a sharp decline under the condition of simulating the tumor microenvironment (pH 6.8+10 mM DTT). The difference was that the particle size of the latter increased to 145±6.6 nm from 127.7±12.2 nm after 4 hours, which could be caused by protonation of the tertiary amine group in RPPssD under acidic conditions.[42] The analysis demonstrated that the preparation achieved the dual-sensitivity property of the initial design, which was conducive to the realization of intelligent drug delivery.

Evaluation of Photothermal and Photodynamic Effects in vitro

The heating process of RPPssD@IR780/DOC under near-infrared laser irradiation was recorded by an infrared thermal imager, and the in vitro photothermal conversion efficiency of RPPssD@IR780/DOC micelles were evaluated. Infrared thermal imaging photos and temperature change curves are shown in Figure 3D and E, respectively. The temperature of the free DOC solution and PBS did not change significantly after continuous laser irradiation (808 nm, 1 W/cm^2, 10 min), while the temperature of the free IR780 and RPPssD@IR780/DOC solution both increased to the highest at 6 min, increasing by 7.8°C and 12.1°C, respectively. In contrast, the RPPssD@IR780/DOC showed a more pronounced and sustained heating process than free IR780. In addition, the photothermal stability results (Figure 3F) of RPPssD@IR780/DOC showed that the rapid degradation of free IR780 after three cycles of irradiation resulted in a rapid decrease in the photothermal conversion efficiency. Conversely, the photothermal conversion efficiency of RPPssD@IR780/DOC changed slightly and was significantly higher than that of free IR780. In addition, the calculated photothermal conversion efficiencies of IR780 and RPPssD@IR780/DOC was 15.4% and 25.6% (Figure 3G). The τ_s of IR780 (Figure 3H) and RPPssD@IR780/DOC (Figure 3I) calculated from linear time data were 252.8 s and 298.5 s in the cooling stage. These results indicated that RPPssD@IR780/DOC had a good photothermal conversion efficiency, while slowing down the degradation of IR780 and maintaining photothermal stability.

DPBF was used to investigate the ability of RPPssD@IR780/DOC to generate ROS. Because DPBF was continuously consumed by reacting with ROS, its remaining amount indicated the amount of ROS produced, reflecting the photodynamic effect. The results are shown in Figure 3J. After irradiating the with near-infrared laser (808 nm, 1 W/cm^2) for 10 minutes, there was no significant change in DPBF absorbance in PBS and the free DOC solution. The absorbance of DPBF in the free IR780 and RPPssD@IR780/DOC groups both decreased significantly, which indicated RPPssD@IR780/DOC effectively produced ROS under irradiation. The photodynamic effect of free IR780 was weaker than that of RPPssD@IR780/DOC, possibly because IR780 had better photostability after being encapsulated by the polymer, which improved the ability to generate singlet oxygen. In addition, the absorbance value of DPBF of DOC was basically unchanged after irradiation, proving that ROS was produced by IR780.

Drug Release of RPPssD@IR780/DOC Micelles Under Different Conditions

According to the design of the RPPssD structure, an acidic environment can promote the expansion of the particle size of RPPssD to release a small amount of drugs and the rupture of the disulfide bonds in the RPPssD structure in the reducing environment can effectively increase the drug release of RPPssD@IR780/DOC. Therefore, by simulating the environment of tumor tissues and tumor cells, RPPssD@IR780/DOC can release drugs faster to treat the lesion. To verify the above conjecture, the release of DOC and IR780 in RPPssD@IR780/DOC under different in vitro conditions was investigated by dialysis (Figure 3K and L). In different pH media (pH=7.4, 6.8, 5.0), the drug release of RPPssD@IR780/DOC increased with the decrease in pH, demonstrating the acid responsiveness of RPPssD@IR780/DOC. At pH 7.4, the cumulative release of IR780 and DOC in RPPssD@IR780/DOC was 41.80% and 37.21%. The cumulative release of IR780 and DOC in RPPssD@IR780/DOC increased to 54.56% and 41.52%, respectively, in the tumor tissue environment (pH 6.8). The cumulative release of the drug at pH 5.0 was much higher than that at pH 7.4 and the cumulative release of IR780 and DOC were 73.03% and 60.27%, respectively. Furthermore, the cumulative release of DOC and IR780 after adding DTT to each pH medium was significantly improved compared to the absence of DTT, which involved the reduction and cleavage of the disulfide bond to release a large amount of drug. The release of DOC and IR780 after adding DTT at pH 7.4 was 48.75% and 60.09%. The release of DOC and IR780 reached 70.65% and 75.16% at pH 6.8 in the presence of DTT. Under the condition of simulating the internal environment (pH 5.0+DTT) of tumor cells, DOC and IR780 were released by 89.72% and 86.28%, respectively. These results indicated that RPPssD in an acidic environment would cause protonation of PBAE, causing the expansion of the micelles, which in turn released more drug than at pH 7.4. When DTT was added to the medium, the breakage of the disulfide bond in the RPPssD structure resulted in the destruction of the micelle structure and in the release of a large amount of drug. In summary, RPPssD@IR780/DOC can effectively encapsulate the drugs and exploit the characteristics of the tumor microenvironment to achieve controlled drug release.

In vitro Biocompatibility Evaluation

In vitro compatibility was examined by a blood compatibility assay and RPPssD@IR780/DOC toxicity to cells. The hemolysis assay was used to study the applicability of RPPssD@IR780/DOC for intravenous administration. Generally speaking, the sample was not hemolyzed when the hemolysis rate was less than 5%.[43] Figure 3J shows that the hemolysis rates of RPPssD@IR780/DOC solutions with a concentration of 15 mg/mL of RPPssD in different volumes were all lower than 5% after adding 2.5 mL of erythrocyte suspension. Similarly, it could be clearly seen (Figure 3M) that the red blood cells from the positive control group with deionized water were hemolyzed. There was no hemolysis observed in the negative control group with PBS. These results indicated that the micelles had a good safety profile in blood and could be used for drug delivery.

Determination of the toxicity of RPPssD in different cells by the CCK-8 method. The PEG in the carrier structure is a biosafety material approved by the FDA and is widely used in the field of drug carriers. PBAE is a class of materials with very low toxicity, which can be degraded into almost nontoxic small molecules of diols and diacids. DSPE is also a lipid molecule with good biocompatibility. The results of the cell experiment here also confirmed the above theory (Figure 3N and O). As the concentration of RPPssD increased, the cell viability of both tumor cells MDA-MB-231 and normal cells L02 cells was greater than 85%, which indicated that RPPssD had low toxicity to normal cells and did not exert any antitumor activity in tumor cells. As RPPssD as a drug carrier, its cell safety can be guaranteed. In summary, RPPssD has good biocompatibility as a drug delivery system.

Cellular Uptake

MDA-MB-231 cells with positive integrin expression and MCF-7 cells with negative integrin expression were used to study cellular uptake of RPPssD. As shown in Figure 4A, the fluorescence intensity of RPPssD@IR780 in the two kinds of cells was higher than that of free IR780 at a different pH, which was because the micelles were more easily absorbed by the cells. The fluorescence intensity of RPPssD@IR780 in MDA-MB-231 cells at pH 6.8 was stronger than that at pH 7.4. This was because the cRGD peptide exposed by RPPssD at pH 6.8 enhanced the ability to actively target MDA-MB-231 cells and

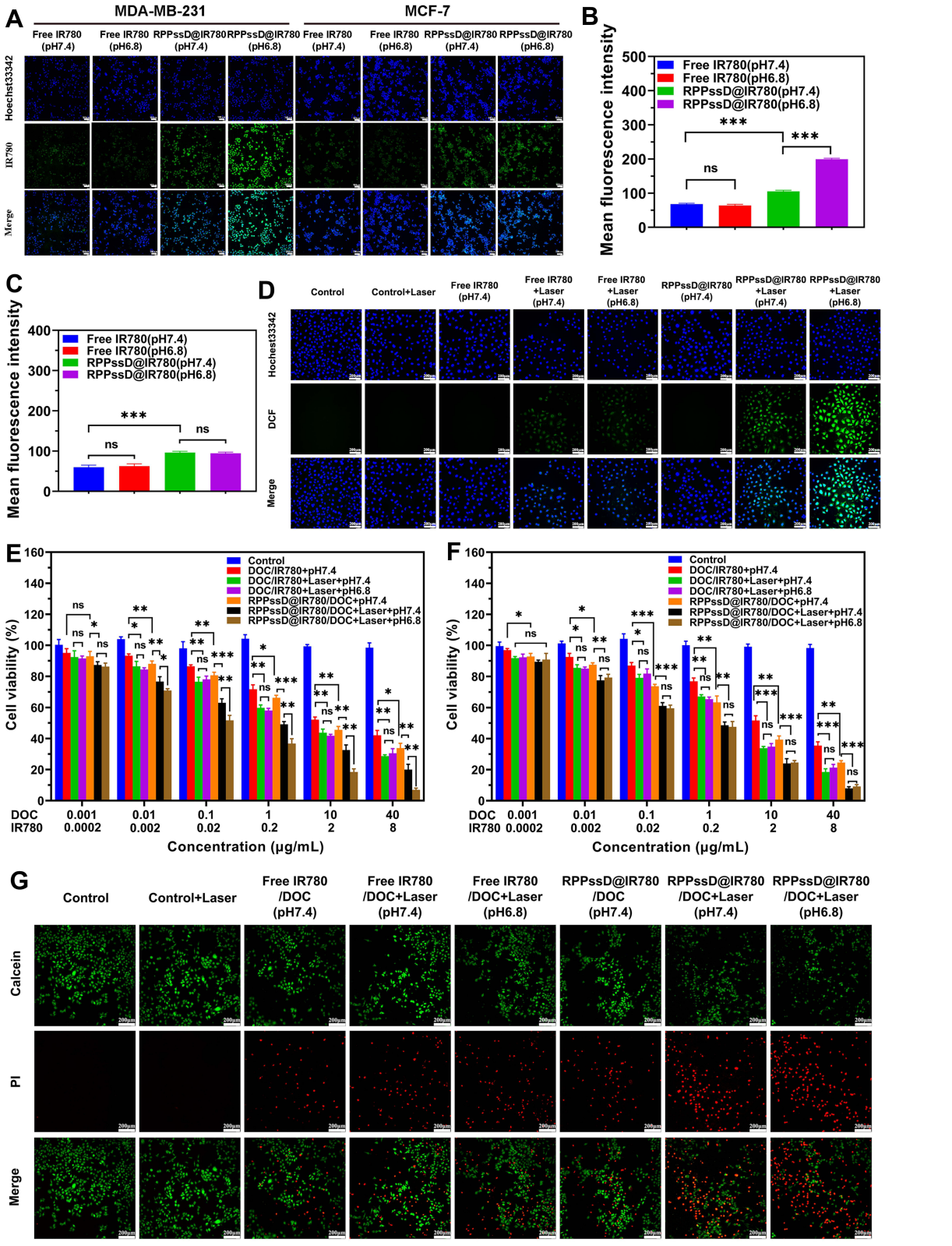

Figure 4 In vitro cellular experiments. (**A**) Uptake of RPPssD@IR780 and IR780 at different pH levels by MDA-MB-231 cells and MCF-7 cells. (**B**) Cell uptake of MDA-MB -231 cells was quantified by Image J. (**C**) The mean fluorescence intensity of the formulation uptake by MCF-7 cells was determined by Image J. (**D**) The ROS in MDA-MB -231 cells after treatment with different samples were detected by DCFH-DA. (**E**) The cytotoxicity of RPPssD@IR780/DOC and free DOC/IR780 for MDA-MB-231 cells. (**F**) The cytotoxicity of RPPssD@IR780/DOC and free DOC/IR780 for MCF-7 cells. (**G**) Fluorescence images of MDA-MB-231 cells after treatment with the formulations (The concentration of DOC and IR780 was 1 μg/mL and 0.2 μg/mL, respectively.) and Calcein/PI staining. (Scale bar = 200 μm). Data are presented as mean ± standard deviation (n = 3), ns > 0.05, *p < 0.05, **p < 0.01 ***p < 0.001.

improved the uptake of micelles by MDA-MB-231. Due to the negative expression of integrin in MCF-7 cells, there was no significant difference in the fluorescence intensity of RPPssD at pH 6.8 and pH 7.4. These results suggested that cRGD could be hidden in the body's circulation but could be exposed to the slightly acidic tumor environment through the pH responsiveness of RPPssD and effectively promoted cellular internalization. The mean fluorescence intensity of the uptake of IR780 and RPPssD@IR780 by MDA-MB-231 cells and MCF-7 cells (Figure 4B and C) achieved the same results.

Cellular ROS Generation

The intracellular ROS generation of RPPssD@IR780 micelles and Free IR780 was measured by DCFH-DA.[44–46] The non-fluorescent DCFH-DA can be converted into green 2',7'-dichlorofluorescein (DCF) by reacting with ROS. As shown in Figure 4D, green fluorescence was hardly observed in the control group and other groups without light. However, both the free IR780 and RPPssD@IR780 groups showed green fluorescence after laser irradiation treatment and the fluorescence intensity of the RPPssD@IR780 group was stronger due to better cellular internalization of micelles. Furthermore, the fluorescence intensity of RPPssD@IR780 micelles at pH6.8 was stronger than at pH 7.4, illustrating that the exposed targeting ligands cRGD of RPPssD@IR780 in an acid environment enhanced its cellular internalization. As a control, no significant differences were observed in the fluorescence intensity of DCF in the free IR780 groups at pH 7.4 or 6.8. These results demonstrated that RPPssD@IR780 could efficiently generate ROS under laser irradiation, enabling photodynamic therapy for tumors.

In vitro Antitumor Activity

To investigate the effects of stimulus-responsive carrier combined with photochemical synergistic therapy, the CCK-8 method was used to detect the toxicity of free IR780/DOC and RPPssD@IR780/DOC to MDA-MB-231 cells with positive expression of the integrin and MCF-7 cells with negative expression of the integrin. As Figure 4E and F demonstrated, the antitumor activity of free DOC/IR780 and RPPssD@IR780/DOC for MDA-MB-231 and MCF-7 was dose-dependent. Because the uptake of micelles by cells was stronger than that of free drugs, the antitumor activity of RPPssD@IR780/DOC was stronger than free DOC/IR780 without laser irradiation. Furthermore, the inhibition rate of free DOC/IR780 and RPPssD@IR780/DOC for MDA-MB-231 and MCF-7 after laser irradiation was significantly increased compared to the nonirradiated groups. The results suggested that the photothermal and photodynamic effects of IR780 after laser irradiation combined with the chemotherapy drug DOC could effectively inhibit tumor cell proliferation, which implied the effectiveness of photochemical synergistic therapy. The targeting ability of RPPssD could be observed from the cytotoxicity of MDA-MB-231 after illumination under different pH conditions. The cytotoxicity of RPPssD@IR780/DOC after laser irradiation at pH 6.8 was higher than that of the laser irradiation groups at pH 7.4, while the cytotoxicity of free DOC/IR780 under these two conditions did not differ significantly. This was because under acidic conditions, the hydrophobic PBAE of RPPssD became hydrophilic while exposed to cRGD with a target effect, which increased the uptake of MDA-MB-231 to drug-loaded micelles and improved the toxicity of the drug to cells. The results in MCF-7 cells also supported the targetability of RPPssD. There was no significant difference in cytotoxicity between RPPssD@IR780/DOC at pH 6.8 and pH 7.4 after irradiation and there was no significant difference in cytotoxicity between free DOC/IR780 under these conditions, which was due to negative expression of the integrin in MCF-7 cells. These results indicated that photochemical synergistic therapy achieves excellent antitumor effects and that RPPssD exhibits specific targeting under acidic conditions, while hiding the target in a normal physiological environment, which represents a potential tumor-targeted drug delivery system.

To more visually examine the toxic effects of RPPssD@IR780/DOC micelles combined with laser irradiation on MDA-MB-231 cells, the Live/Dead staining kit was used to stain MDA-MB-231 cells from different treatment groups, followed by observation of cell survival under fluorescence microscopy. Live and dead cells exhibit green and red fluorescence, respectively, under a fluorescence microscope. The fluorescence microscope images of MDA-MB-231 cells in different experimental groups after live/dead cell staining are shown in Figure 4G. In the control groups, the cells showed green fluorescence and almost completely survived with or without light. In the free drug group, fewer dead cells were observed, indicating that the cytotoxicity of free drugs on cells was not obvious. However, the toxicity of the free drug groups to cells was significantly enhanced after laser irradiation. Moreover, the ratio of dead cells in the RPPssD@IR780/DOC micelles

groups with or without laser irradiation was significantly higher than that in the free drug groups. In addition, RPPssD@IR780/DOC micelles were more cytotoxic in an acidic environment than at pH7.4, while the free drug group did not show any difference in cytotoxicity due to changes in pH. These results showed that RPPssD@IR780/DOC micelles combined with laser irradiation exerted a significant antitumor effect. Furthermore, the antitumor effect of the RPPssD@IR780/DOC micelles improved on exposure of the cRGD peptides to acidic conditions. This further shows that RPPssD@IR780/DOC micelles have great potential to realize combined photochemical treatment for tumors.

Infrared Light-Induced Photothermal Effect in vivo

The photothermal effect of RPPssD@IR780/DOC was further demonstrated by recording the change in tumor surface temperature by infrared thermography within 6 min of laser irradiation (1 W/cm^2, 6 min) after 8 h of control treatment (saline), DOC/IR780 and RPPssD@IR780/DOC injections to tumor-bearing mice. As described in Figure 5A and B, the tumor surface temperature of the RPPssD@IR780/DOC group increased rapidly by 16.1°C while the IR780 group increased by 8.8°C after NIR laser irradiation. This is due to the fact that RPPssD@IR780/DOC can enrich the drug in the tumor through passive targeting and RGD-mediated active targeting, thus exhibiting better in vivo photothermal effects. In comparison, the change in tumor surface temperature in the saline group appeared to be insignificant. These results suggested that RPPssD@IR780/DOC offers a new possibility for photothermal treatment of tumors.

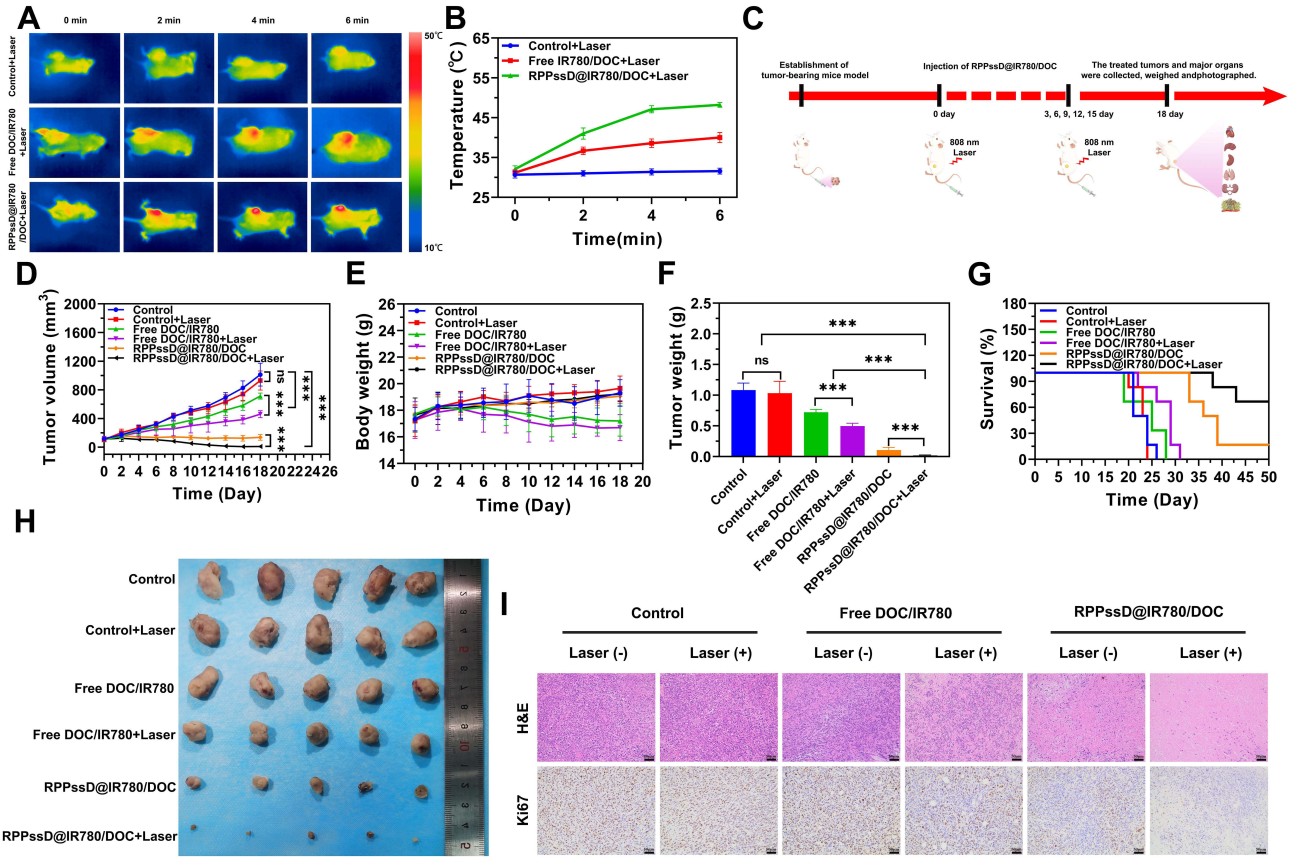

Figure 5 Evaluation of in vivo thermal activity and antitumor effect. (**A**) Infrared thermograms of tumor-bearing mice after infrared laser irradiation with saline injection into the tail vein, free DOC/IR780, and RPPssD@IR780/DOC, respectively. (**B**) Change curves of tumor surface temperature in different groups of tumor-bearing mice after infrared laser irradiation. (**C**) Experimental protocol for in vivo photochemical therapy of tumors. (**D**) Tumor volume variation curves of tumor-bearing mice in each group. (**E**) The body weight variation of tumor-bearing mice in each group. (**F**) Tumor weight of tumor-bearing mice in each group. (**G**) Survival curves of tumor-bearing mice in each group. (**H**) Photographs of tumor tissues after treatment in different groups. (**I**) The H&E staining and Ki67 immunohistochemical analysis of tumor tissues from tumor-bearing mice in each treatment group (Scale bar=50 μm). Data are presented as mean ± standard deviation (n = 6), ns > 0.05, ***p < 0.001.

In vivo Photochemical Combination Therapy Effect on Tumor

The low toxicity, targeting ability, and outstanding in vitro antitumor activity of RPPssD@IR780/DOC prompted us to further evaluate the antitumor efficacy in MDA-MB-231 cell tumor-bearing mice. The in vivo antitumor assay workflow is illustrated in Figure 5C. The changes in tumor volume during treatment in each group are shown in Figure 5D. The DOC/IR780 group, DOC/IR780+Laser group, RPPssD@IR780/DOC group, and RPPssD@IR780/DOC+Laser group all exhibited different degrees of tumor growth inhibition compared to the control group. Both the DOC/IR780 group and the RPPssD@IR780/DOC group showed higher inhibition rates for tumors in response to exposure laser therapy compared to the absence of laser irradiation, which indicated the effectiveness of the photochemical combination for tumor treatment. In particular, the specific targeting effect of RPPssD@IR780/DOC resulted in a more pronounced tumor suppression effect in the RPPssD@IR780/DOC group with or without laser than in the free DOC/IR780 group. At the end of treatment, the mice were killed to collect tumors for photographing and weighing. As Figure 5F demonstrated, the tumor weights and photos of each group also illustrated the excellent antitumor effect of RPPssD@IR780/DOC under laser irradiation. Tumor tissue images (Figure 5H) of MDA-MB-231 tumor-bearing mice from each treatment group confirmed the same results. The tumor inhibition ratio (Figure S10) of the RPPssD@IR780/DOC group after laser irradiation was 2.95 times that of the free drug group.

Notably, the systemic toxicity of DOC caused a slight decrease in body weight (Figure 5E) in mice in the free drug group with or without light. In contrast, the mice in the RPPssD@IR780/DOC group showed no significant change in body weight during the treatment period with or without laser irradiation, indicating the low systemic toxicity of RPPssD@IR780/DOC micelles. Survival experiments confirmed that RPPssD@IR780/DOC micelles significantly improved the survival of tumor-bearing mice. Figure 5G shows the survival rate of mice in each treatment group, which indicated that mice in the RPPssD@IR780/DOC group had the highest survival rate of 66.7% within 50 days after treatment. To further investigate antitumor effects, H&E and Ki67 staining (Figure 5I) was performed on tumor tissue sections. H&E staining demonstrated that the cells in the tumor tissues were evenly distributed with intact nuclei and dense tissues, and no obvious damage was seen in the control group with or without light. Conversely, each of the other administration groups exhibited significant apoptosis of tumor cells with nuclear pyknosis and cell membrane rupture. Especially in the RPPssD@IR780/DOC group after near-infrared light irradiation, apoptosis was most evident with incomplete cell morphology and the formation of cell-free necrotic areas. Furthermore, Ki67 was used to assess tumor cell proliferation in each group. Consistent with the results of the H&E staining, the Ki67 level of RPPssD@IR780/DOC was the lowest among the groups under near-infrared light irradiation, indicating the effective inhibition of tumor cell proliferation. These results confirmed that RPPssD@IR780/DOC is an effective antitumor micelle by inhibiting tumor cell proliferation and inducing tumor cell apoptosis to achieve photochemical therapy of tumors while reducing the systemic toxicity of drugs.

In vivo Biosafety Assessment

Biosafety is a prerequisite of nanomedicines for disease treatment. The biosafety of RPPssD@IR780/DOC micelles were evaluated by H&E staining and serum biochemical analysis. The results of H&E staining showed that, compared to the control group, there were no obvious abnormalities or lesions in the heart, liver, spleen, lung, or kidney of each treatment group. The structure of each organ was normal, no obvious congestion or expansion of blood vessels was observed, and no significant inflammatory or hemorrhagic reaction was found in the tissue, indicating that the toxicity of RPPssD@IR780/DOC micelles to the main organs of mice was negligible (Figure 6A). The hepatotoxicity (ALT, AST, ALP), nephrotoxicity (BUN, CRE), cardiotoxicity (CK) and hematological indices of RPPssD@IR780/DOC were studied by serum biochemical indices and routine blood analysis (Figure 6B–L). Compared with the control group, no significant changes in liver, kidney, and cardiac function indices were observed in each treatment group. All indexes were at or near normal healthy levels. Notably, the possible myelosuppressive effect caused by DOC was observed in the free DOC/IR780 group with or without laser irradiation, as evidenced by a certain degree of decrease in both WBC and NEU% levels, which was not observed in the RPPssD@IR780/DOC group with or without laser irradiation. These results demonstrated that RPPssD@IR780/DOC micelles are effective in reducing the systemic toxicity of chemotherapeutic agents and excellent biosafety in photochemotherapy.

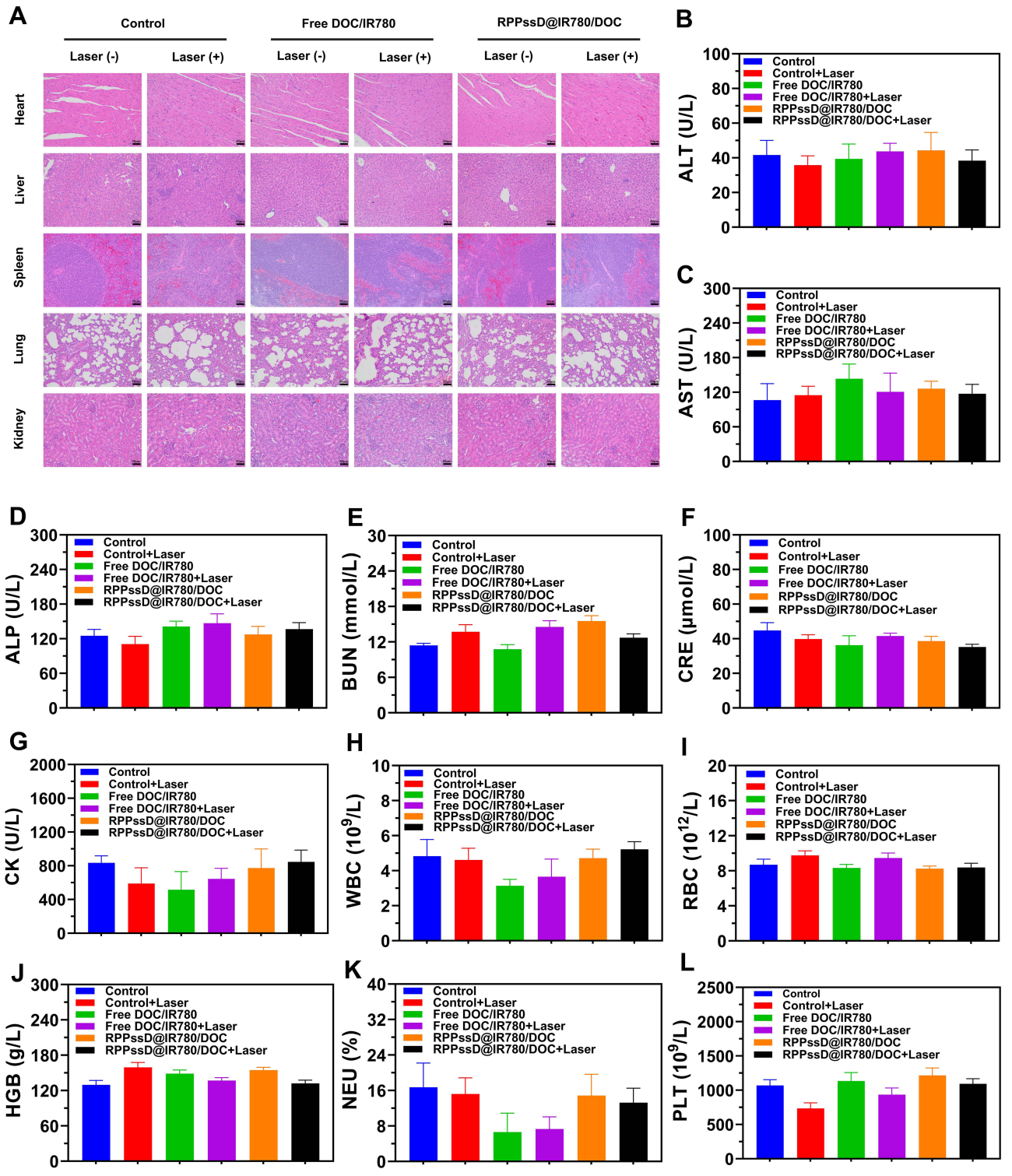

Figure 6 Biosafety of RPPssD@IR780/DOC micelles. (**A**) H&E staining of major organ tissues (heart, liver, spleen, lung, and kidney) of tumor-bearing mice in each treatment group. (Scale bar=50 μm). (**B**–**L**) Routine and blood biochemical parameters of mice after tail vein injection of saline, free DOC/IR780 and RPPssD@IR780/DOC with or without laser irradiation. ALT, AST, and ALP were used to assess liver injury, renal injury was estimated by BUN and CRE, while CK was an indicator of myocardial injury. In addition, WBC, RBC, HGB, NEU% and PLT were used in blood routine to evaluate the toxicity of the drug in mice. Data are presented as mean ± standard deviation (n = 6).

Conclusions

We have successfully developed a pH/reduction dual-activity micelle RPPssD with concealable targeting ligands for encapsulating DOC and IR780 for photochemical treatment of tumors. The low CMC of RPPssD enables it to self-assemble to form stable micelles in water. To achieve photochemical treatment of tumors, DOC and IR780 were encapsulated inside the RPPssD micelles with uniform particle size using a thin film dispersion method. The formed RPPssD@IR780/DOC can effectively improve the solubility of DOC and IR780, and they have good stability in PBS and DMEM medium containing 10% FBS. Furthermore, the PBAE in the RPPssD block polymer could change from hydrophobic to hydrophilic properties under acidic conditions, thereby ensuring that the cRGD peptide in the micelles can be covered by a PEG shell with masking function under physiological conditions. After reaching the tumor site, the micelles increased in size and exposed targeted cRGD peptides to enhance retention time in the tumor and cellular internalization of the micelles. When the micelles enter tumor cells, the disulfide bonds in RPPssD were affected by the high expression of GSH in the cells to release the active drugs DOC and IR780, which can generate a large amount of ROS and heat after laser irradiation to kill the cells. Moreover, the results of in vitro and in vivo experiments demonstrate the efficacy and biosafety of RPPssD@IR780/DOC for tumor photochemical therapy, which is a promising tumor-targeted drug delivery system.

Abbreviations

DOC, docetaxel; IR780, IR-780 iodide; PEG, polyethylene glycol; PBAE, poly(β-amino esters); DSPE, distearoyl phosphatidylethanolamine; ROS, reactive oxygen species; RGD, cyclic Arg-Gly-Asp; PDT, photodynamic therapy; PTT, photothermal therapy; PS, photosensitizer; EPR, enhanced permeability and penetration; GSH, glutathione; DTT, dithiothreitol; NIR, Near-infrared; CMC, critical micelle concentration; PDI, Polymer dispersity index; DL, drug loading; EE, encapsulation efficiency; DPBF, 3-diphenylisobenzofuran; OD, optical density; CCK-8, cell counting kit-8; DCFH-DA, 2′,7′-Dichlorofluorescin diacetate; DCF, 2',7'-dichlorofluorescein; H&E, hematoxylin-eosin; TEM, transmission electron microscope; DMEM, Dulbecco's modified Eagle's medium; FBS, Fetal Bovine Serum; GPC, gel permeation chromatography.

Supporting Information

The Supporting Information contains details on experimental materials, cell culture conditions, synthesis of the RPPssD polymer, the protocol for the establishment of the animal model, ^{1}H NMR spectroscopy and analysis of RPPssD, GPC of RPPssD, content standard curve of DOC and IR780, solubility evaluation of DOC and IR780, tumor inhibition rate of each group of mice in this paper.

Ethics Statement

The experimental procedures used in this study were approved by the Guidelines for Care and Use of Laboratory Animals of Nanjing Tech University and experiments were approved by the Animal Ethics Committee of Jiangsu Center for Safety Evaluation of Drugs.

Acknowledgments

This work was supported by the Science and Technology Planning Project of Jiangsu Province of China BE2019738 and Natural Science Foundation of the Higher Education Institutions of Jiangsu Province of China 20KJB630004 .

Disclosure

The authors report no conflicts of interest in this work.

References

1. Bray F, Ferlay J, Soerjomataram I, Siegel RL, Torre LA, Jemal A. Global cancer statistics 2018: GLOBOCAN estimates of incidence and mortality worldwide for 36 cancers in 185 countries. *CA Cancer J Clin*. 2018;68(6):394–424. doi:10.3322/caac.21492
2. Mansouri V, Beheshtizadeh N, Gharibshahian M, Sabouri L, Varzandeh M, Rezaei N. Recent advances in regenerative medicine strategies for cancer treatment. *Biomed Pharmacother*. 2021;141:111875. doi:10.1016/j.biopha.2021.111875

3. Sedighi M, Zahedi Bialvaei A, Hamblin MR, et al. Therapeutic bacteria to combat cancer; current advances, challenges, and opportunities. *Cancer Med*. 2019;8(6):3167–3181. doi:10.1002/cam4.2148
4. Gao D, Guo X, Zhang X, et al. Multifunctional phototheranostic nanomedicine for cancer imaging and treatment. *Mater Today Bio*. 2020;5:100035. doi:10.1016/j.mtbio.2019.100035
5. Alves SR, Calori IR, Tedesco AC. Photosensitizer-based metal-organic frameworks for highly effective photodynamic therapy. *Mater Sci Eng C Mater Biol Appl*. 2021;131:112514. doi:10.1016/j.msec.2021.112514
6. Kumar AVP, Dubey SK, Tiwari S, et al. Recent advances in nanoparticles mediated photothermal therapy induced tumor regression. *Int J Pharm*. 2021;606:120848.
7. Zhang Y, Wang B, Zhao R, Zhang Q, Kong X. Multifunctional nanoparticles as photosensitizer delivery carriers for enhanced photodynamic cancer therapy. *Mater Sci Eng C Mater Biol Appl*. 2020;115:111099. doi:10.1016/j.msec.2020.111099
8. Hak A, Ravasaheb Shinde V, Rengan AK. A review of advanced nanoformulations in phototherapy for cancer therapeutics. *Photodiagnosis Photodyn Ther*. 2021;33:102205. doi:10.1016/j.pdpdt.2021.102205
9. Ghosh S, Carter KA, Lovell JF. Liposomal formulations of photosensitizers. *Biomaterials*. 2019;218:119341. doi:10.1016/j.biomaterials.2019.119341
10. Moghassemi S, Dadashzadeh A, Azevedo RB, Feron O, Amorim CA. Photodynamic cancer therapy using liposomes as an advanced vesicular photosensitizer delivery system. *J Control Release*. 2021;339:75–90. doi:10.1016/j.jconrel.2021.09.024
11. Raj S, Khurana S, Choudhari R, et al. Specific targeting cancer cells with nanoparticles and drug delivery in cancer therapy. *Semin Cancer Biol*. 2021;69:166–177. doi:10.1016/j.semcancer.2019.11.002
12. Wang X, Yang T, Yu Z, et al. Intelligent gold nanoparticles with oncogenic microrna-dependent activities to manipulate tumorigenic environments for synergistic tumor therapy. *Adv Mater*. 2022;34(15):e2110219. doi:10.1002/adma.202110219
13. Lee K, Lee H, Bae KH, Park TG. Heparin immobilized gold nanoparticles for targeted detection and apoptotic death of metastatic cancer cells. *Biomaterials*. 2010;31(25):6530–6536. doi:10.1016/j.biomaterials.2010.04.046
14. Xu F, Huang X, Wang Y, Zhou S. A size-changeable collagenase-modified nanoscavenger for increasing penetration and retention of nanomedicine in deep tumor tissue. *Adv Mater*. 2020;32(16):e1906745. doi:10.1002/adma.201906745
15. Liang P, Huang X, Wang Y, et al. Tumor-microenvironment-responsive nanoconjugate for synergistic antivascular activity and phototherapy. *ACS Nano*. 2018;12(11):11446–11457. doi:10.1021/acsnano.8b06478
16. Ren LL, Nie JF, Wei J, et al. RGD-targeted redox responsive nano micelles: co-loading docetaxel and indocyanine green to treat the tumor. *Drug Deliv*. 2021;28(1):2024–2032. doi:10.1080/10717544.2021.1977425
17. Chen G, Zheng Q, Dai J, et al. Reduction-sensitive mixed micelles based on mPEG-SS-PzLL/TPGS to enhance anticancer efficiency of doxorubicin. *React Func Polym*. 2022;174:105242. doi:10.1016/j.reactfunctpolym.2022.105242
18. Madathiparambil Visalakshan R, Gonzalez Garcia LE, Benzigar MR, et al. The influence of nanoparticle shape on protein Corona formation. *Small*. 2020;16(25):e2000285. doi:10.1002/smll.202000285
19. Yang Y, Wu H, Liu B, Liu Z. Tumor microenvironment-responsive dynamic inorganic nanoassemblies for cancer imaging and treatment. *Adv Drug Deliv Rev*. 2021;179:114004. doi:10.1016/j.addr.2021.114004
20. Tekie FSM, Hajiramezanali M, Geramifar P, et al. Controlling evolution of protein Corona: a prosperous approach to improve chitosan-based nanoparticle biodistribution and half-life. *Sci Rep*. 2020;10(1):9664. doi:10.1038/s41598-020-66572-y
21. Xiao W, Gao H. The impact of protein Corona on the behavior and targeting capability of nanoparticle-based delivery system. *Int J Pharm*. 2018;552(1–2):328–339. doi:10.1016/j.ijpharm.2018.10.011
22. Fam SY, Chee CF, Yong CY, Ho KL, Mariatulqabtiah AR, Tan WS. Stealth coating of nanoparticles in drug-delivery systems. *Nanomaterials*. 2020;10(4):787. doi:10.3390/nano10040787
23. Huang W, Xiao G, Zhang Y, Min W. Research progress and application opportunities of nanoparticle-protein Corona complexes. *Biomed Pharmacother*. 2021;139:111541. doi:10.1016/j.biopha.2021.111541
24. Zhang H, Dong S, Zhang S, et al. pH-responsive lipid polymer hybrid nanoparticles (LPHNs) based on poly (β-amino ester) as a promising candidate to resist breast cancers. *J Drug Deliv Sci Technol*. 2021;61:102102.
25. Mo Z, Qiu M, Zhao K, et al. Multifunctional phototheranostic nanoplatform based on polydopamine-manganese dioxide-IR780 iodide for effective magnetic resonance imaging-guided synergistic photodynamic/photothermal therapy. *J Colloid Interface Sci*. 2022;611:193–204. doi:10.1016/j.jcis.2021.12.071
26. Van Hove I, Hu TT, Beets K, et al. Targeting RGD-binding integrins as an integrative therapy for diabetic retinopathy and neovascular age-related macular degeneration. *Prog Retin Eye Res*. 2021;85:100966. doi:10.1016/j.preteyeres.2021.100966
27. Zhang L, Chou CP, Moo-Young M. Disulfide bond formation and its impact on the biological activity and stability of recombinant therapeutic proteins produced by Escherichia coli expression system. *Biotechnol Adv*. 2011;29(6):923–929. doi:10.1016/j.biotechadv.2011.07.013
28. Salem JK, El-Nahhal IM, Salama SF. Determination of the critical micelle concentration by absorbance and fluorescence techniques using fluorescein probe. *Chem Phys Lett*. 2019;730:445–450. doi:10.1016/j.cplett.2019.06.038
29. Zhou M, Yi Y, Liu L, et al. Polymeric micelles loading with ursolic acid enhancing anti-tumor effect on hepatocellular carcinoma. *J Cancer*. 2019;10(23):5820–5831. doi:10.7150/jca.30865
30. Xu Y, Liu D, Hu J, Ding P, Chen M. Hyaluronic acid-coated pH sensitive poly (beta-amino ester) nanoparticles for co-delivery of embelin and TRAIL plasmid for triple negative breast cancer treatment. *Int J Pharm*. 2020;573:118637. doi:10.1016/j.ijpharm.2019.118637
31. Wang Q, Zou C, Wang L, et al. Doxorubicin and adjudin co-loaded pH-sensitive nanoparticles for the treatment of drug-resistant cancer. *Acta Biomater*. 2019;94:469–481. doi:10.1016/j.actbio.2019.05.061
32. Fu S, Rempson CM, Puche V, Zhao B, Zhang F. Construction of disulfide containing redox-responsive polymeric nanomedicine. *Methods*. 2022;199:67–79. doi:10.1016/j.ymeth.2021.12.011
33. Wang S, Yang Y, Wu H, et al. Thermosensitive and tum or microenvironment activated nanotheranostics for the chemodynamic/photothermal therapy of colorectal tumor. *J Colloid Interface Sci*. 2022;612:223–234. doi:10.1016/j.jcis.2021.12.126
34. Zhang L, He G, Yu Y, et al. Design of biocompatible chitosan/polyaniline/laponite hydrogel with photothermal conversion capability. *Biomolecules*. 2022;12(8):1089. doi:10.3390/biom12081089

35. Zhang Y, Du X, Liu S, et al. NIR-triggerable ROS-responsive cluster-bomb-like nanoplatform for enhanced tumor penetration, phototherapy efficiency and antitumor immunity. *Biomaterials*. 2021;278:121135. doi:10.1016/j.biomaterials.2021.121135
36. Sun B, Luo C, Yu H, et al. Disulfide bond-driven oxidation- and reduction-responsive prodrug nanoassemblies for cancer therapy. *Nano Lett*. 2018;18(6):3643–3650. doi:10.1021/acs.nanolett.8b00737
37. Zhang Y, Yang D, Chen H, et al. Reduction-sensitive fluorescence enhanced polymeric prodrug nanoparticles for combinational photothermal-chemotherapy. *Biomaterials*. 2018;163:14–24. doi:10.1016/j.biomaterials.2018.02.023
38. He X, Chen X, Liu L, et al. Sequentially triggered nanoparticles with tumor penetration and intelligent drug release for pancreatic cancer therapy. *Adv Sci*. 2018;5(5):1701070. doi:10.1002/advs.201701070
39. Bauer K, Mierke C, Behrens J. Expression profiling reveals genes associated with transendothelial migration of tumor cells: a functional role for alphavbeta3 integrin. *Int J Cancer*. 2007;121(9):1910–1918. doi:10.1002/ijc.22879
40. Singh C, Shyanti RK, Singh V, Kale RK, Mishra JPN, Singh RP. Integrin expression and glycosylation patterns regulate cell-matrix adhesion and alter with breast cancer progression. *Biochem Biophys Res Commun*. 2018;499(2):374–380. doi:10.1016/j.bbrc.2018.03.169
41. Rivas Mercado E, Neri Castro E, Benard Valle M, et al. Disintegrins extracted from totonacan rattlesnake (Crotalus totonacus) venom and their anti-adhesive and anti-migration effects on MDA-MB-231 and HMEC-1 cells. *Toxicol In vitro*. 2020;65:104809. doi:10.1016/j.tiv.2020.104809
42. Lin Y-K, Wang S-W, Lee R-S. Reductive responsive hyaluronic acid conjugated S-nitrothiol prodrugs as drug carriers. *Int J Polym Mater Polym Biomaterial*. 2021;711–14.
43. Zhou Y, Li N, Qiu Z, et al. Superior anti-neoplastic activities of triacontanol-PEG conjugate: synthesis, characterization and biological evaluations. *Drug Deliv*. 2018;25(1):1546–1559. doi:10.1080/10717544.2018.1477864
44. Hao Y, Chen Y, He X, et al. Polymeric nanoparticles with ROS-responsive prodrug and platinum nanozyme for enhanced chemophotodynamic therapy of colon cancer. *Adv Sci*. 2020;7(20):2001853. doi:10.1002/advs.202001853
45. Refsnes M, Skuland T, Lilleaas E, Ovrevik J, Lag M. Concentration-dependent cytokine responses of silica nanoparticles and role of ROS in human lung epithelial cells. *Basic Clin Pharmacol Toxicol*. 2019;125(3):304–314. doi:10.1111/bcpt.13221
46. Chu B, Qu Y, He X, et al. ROS-responsive camptothecin prodrug nanoparticles for on-demand drug release and combination of chemotherapy and photodynamic therapy. *Adv Funct Mater*. 2020;30:52. doi:10.1002/adfm.202005918